

Using the Bright Ultra-Hard *XMM-Newton* Survey to define an IR selection of luminous AGN based on WISE colours

S. Mateos^{1,2*}, A. Alonso-Herrero^{1†}, F. J. Carrera¹, A. Blain², M. G. Watson², X. Barcons¹, V. Braitto³, P. Severgnini⁴, J. L. Donley⁵ and D. Stern⁶

¹ Instituto de Física de Cantabria (CSIC-Universidad de Cantabria), 39005, Santander, Spain

² Physics and Astronomy, University of Leicester, University Road, Leicester LE1 7RH, UK

³ Istituto Nazionale di Astrofisica - Osservatorio Astronomico di Brera, Via Bianchi 46 I-23807 Merate (LC), Italy

⁴ INAF-Osservatorio Astronomico di Brera, via Brera 28, 20121 Milano, Italy

⁵ Los Alamos National Laboratory, Los Alamos, NM 87545, USA

⁶ Jet Propulsion Laboratory, California Institute of Technology, Pasadena, CA 91109, USA

Accepted 2012 July 31. Received 2012 July 27; in original form 2012 June 26

ABSTRACT

We present a highly complete and reliable mid-infrared (MIR) colour selection of luminous AGN candidates using the 3.4, 4.6, and 12 μm bands of the WISE survey. The MIR colour wedge was defined using the wide-angle Bright Ultra-Hard *XMM-Newton* Survey (BUXS), one of the largest complete flux-limited samples of bright ($f_{4.5-10\text{keV}} > 6 \times 10^{-14} \text{erg s}^{-1} \text{cm}^{-2}$) “ultra-hard” (4.5–10 keV) X-ray selected AGN to date. BUXS includes 258 objects detected over a total sky area of 44.43 deg² of which 251 are spectroscopically identified and classified, with 145 being type-1 AGN and 106 type-2 AGN. Our technique is designed to select objects with red MIR power-law spectral energy distributions (SED) in the three shortest bands of WISE and properly accounts for the errors in the photometry and deviations of the MIR SEDs from a pure power-law. The completeness of the MIR selection is a strong function of luminosity. At $L_{2-10\text{keV}} > 10^{44} \text{erg s}^{-1}$, where the AGN is expected to dominate the MIR emission, 97.1^{+2.2%}_{-4.8%} and 76.5^{+13.3%}_{-18.4%} of the BUXS type-1 and type-2 AGN meet the selection. Our technique shows one of the highest reliability and efficiency of detection of the X-ray selected luminous AGN population with WISE amongst those in the literature. In the area covered by the BUXS survey our selection identifies 2755 AGN candidates detected with SNR ≥ 5 in the three shorter wavelength bands of WISE with 38.5% having a detection at 2–10 keV X-ray energies. We also analyzed the possibility of including the 22 μm WISE band to select AGN candidates, but neither the completeness nor the reliability of the selection improves. This is likely due to both the significantly shallower depth at 22 μm compared with the first three bands of WISE and star-formation contributing to the 22 μm emission at the WISE 22 μm sensitivity.

Key words: galaxies: active-quasars: general-infrared: galaxies

1 INTRODUCTION

There is strong observational evidence that active galactic nuclei (AGN) play an important role in the formation and growth of galaxies (e.g. Magorrian et al. 1998). Most super-massive black hole growth takes place during an obscured quasar phase, as suggested by the integrated energy density

of the cosmic X-ray background (Fabian & Iwasawa 1999). To understand the evolution of galaxies and to trace the energy output due to accretion and its cosmological evolution, it is critical to map the history of obscured accretion.

X-ray surveys with *XMM-Newton* and *Chandra* at energies < 10 keV are sensitive to all but the most heavily obscured AGN (e.g. Della Ceca et al. 2008). In Compton-thick AGN (rest-frame column densities exceeding $N_{\text{H}} \simeq 1.5 \times 10^{24} \text{cm}^{-2}$) the observed flux below 10 keV

*E-mail: mateos@ifca.unican.es

†Augusto G. Linares Senior Research Fellow

can be as low as a few % of the intrinsic nuclear flux. In the Compton-thick regime the high energy photons that survive the photoelectric absorption get scattered in the absorber losing part of their energy (Compton down-scattering). This is an important effect that can significantly suppress the transmitted continuum (Matt 2002; Murphy & Yaqoob 2009; Yaqoob et al. 2010). The ongoing Swift/BAT and INTEGRAL/IBIS all-sky surveys at energies 15-200 keV are providing the least biased samples of absorbed AGN in the local Universe (e.g. Bird et al. 2007; Tueller et al. 2008; Winter et al. 2009; Burlon et al. 2011). However, even these surveys are biased against the most heavily absorbed Compton-thick AGN (Burlon et al. 2011).

Surveys at mid-infrared (hereafter MIR) wavelengths ($\gtrsim 5\mu\text{m}$) are much less affected by extinction since the obscuring dust re-emits the nuclear optical-to-X-ray radiation at infrared wavelengths. Clumpy torus models predict nearly isotropic emission in the MIR at wavelengths $\gtrsim 12\mu\text{m}$ (Nenkova et al. 2008). Thus, MIR-based surveys (or the combination of MIR and data at shorter wavelengths) can potentially trace the elusive obscured accretion missed by hard X-ray surveys (e.g. Daddi et al. 2007; Fiore et al. 2008; Georgantopoulos et al. 2008; Fiore et al. 2009; Severgnini et al. 2012). For example, it has been claimed that objects showing excess emission at $\sim 24\mu\text{m}$ over that expected from star formation, termed "infrared-excess galaxies", might host heavily obscured and Compton-thick AGN (e.g. Fiore et al. 2008; Fiore et al. 2009). However the exact contribution of heavily obscured AGN to the infrared-excess galaxy population remains an open issue (e.g. Alexander et al. 2011). Several MIR-based AGN selection techniques have been developed with data from the Spitzer Space Telescope Infrared Array Camera (IRAC; Fazio et al. 2004) using colours and power-law selection (Lacy et al. 2004; Stern et al. 2005; Alonso-Herrero et al. 2006; Donley et al. 2008, 2012). These techniques are very effective and reliable. Galaxies dominated by AGN emission typically exhibit a characteristic red power-law spectral energy distribution (SED) in the MIR ($f_\nu \propto \nu^\alpha$ with $\alpha \leq -0.5$; Alonso-Herrero et al. 2006). Thus, MIR power-law selection provides the cleanest samples of luminous AGN (e.g. Donley et al. 2008). However, this technique is very sensitive to the reliability of the estimated photometric errors (Donley et al. 2012).

The Wide-field Infrared Survey Explorer (WISE) has now completed the first sensitive (~ 100 - $1000\times$ deeper than IRAS) coverage of the entire sky in the MIR¹ (Wright et al. 2010). Several colour-based regions, aimed at identifying luminous AGN, have already been proposed. These works have shown that WISE can robustly separate AGN from normal galaxies and stars (e.g. Assef et al. 2010; Jarrett et al. 2011; Stern et al. 2012). WISE will be extremely efficient in identifying the rare highly luminous AGN up to the crucial epoch when the accretion power of the Universe peaked ($z \sim 1$ - 2). The all-sky WISE survey will complement the deep Spitzer surveys, aimed to characterize the accretion phenomenon in the distant Universe.

This paper presents a highly reliable and complete MIR-based colour selection of AGN with WISE. Our technique

is designed to select objects with red MIR power-law SEDs and properly accounts for the estimated typical errors in the photometry and deviations of the MIR SEDs from a pure power-law. The AGN wedge is defined using the wide-angle Bright Ultra-hard *XMM-Newton* Survey (BUXS; Mateos et al. 2012c, in preparation). This survey is one of the largest complete flux-limited samples of bright "ultra-hard" (4.5-10 keV) X-ray selected AGN to date. Surveys such as BUXS are extremely efficient in selecting AGN bright enough for reliable optical identifications and for detailed studies of their properties and evolution (e.g. HBS28, Caccianiga et al. 2004; HBSS, Della Ceca et al. 2008). BUXS covers the region of the AGN redshift-luminosity parameter space that WISE will sample. Thus, BUXS offers a unique opportunity to define a highly complete and reliable MIR-based AGN selection with WISE. Thanks to the optical spectroscopic identifications available for $\sim 97\%$ of the BUXS objects, and the high quality X-ray spectra, we have maximized the completeness of our MIR selection without compromising its reliability. In a forthcoming paper we will present and discuss the main properties of the optical/near-IR/MIR SEDs of the AGN in BUXS (Mateos et al. 2012c, in preparation).

This paper is organized as follows. Sections 2 and 3 briefly summarize the data sets. In Section 4 we present our MIR selection of AGN candidates using the three shorter wavelength bands of WISE and the complete four bands, respectively and we discuss the completeness of the selection. We show the reliability of our AGN selection in Section 5. The results are summarized in Section 6. Throughout this paper errors are 90% confidence for a single parameter and we assume $\Omega_M = 0.3$, $\Omega_\Lambda = 0.7$ and $H_0 = 70 \text{ km s}^{-1} \text{ Mpc}^{-1}$.

2 THE WISE INFRARED SURVEY

WISE observed the entire sky in the MIR, achieving 5σ point source sensitivities better than 0.08, 0.11, 1, and 6 mJy at 3.4, 4.6, 12, and $22 \mu\text{m}$, respectively. The angular resolution is $6.1''$, $6.4''$, $6.5''$, and $12.0''$ (FWHM), respectively, and the astrometric precision for high signal-to-noise (hereafter SNR) sources is better than $0.15''$ (Wright et al. 2010). We use here the March 2012 publicly available All-Sky Data Release that covers $>99\%$ of the sky and incorporates the best available calibrations and data reduction algorithms (Cutri et al. 2012).

In what follows we compute flux densities in the WISE bands using profile fitting photometry and the magnitude zero points of the Vega system: $F_\nu(\text{iso}) = 309.124 \text{ Jy}$, 171.641 Jy , 30.988 Jy , and 8.346 Jy for 3.4, 4.6, 12, and $22 \mu\text{m}$, respectively. These values are computed with the flux correction factors that correspond to a power-law spectrum ($f_\nu \propto \nu^\alpha$) with spectral index $\alpha = -1$ presented in Wright et al. (2010). We note that using the flux correction factors that correspond to constant power-law spectra the difference in the computed flux densities would be less than 0.2% at 3.4, 4.6, and $22 \mu\text{m}$ and $\sim 2\%$ at $12 \mu\text{m}$. We added a 1.5% uncertainty to the catalogued flux errors in all bands to account for the overall systematic uncertainty from the Vega spectrum in the flux zeropoints. To account for the existing discrepancy between the red and blue calibrators used for the conversion from magnitudes to Janskys, an additional 10% uncertainty was added to the $12\mu\text{m}$ and $22\mu\text{m}$ fluxes (Wright

¹ <https://ceres.ipac.caltech.edu/>

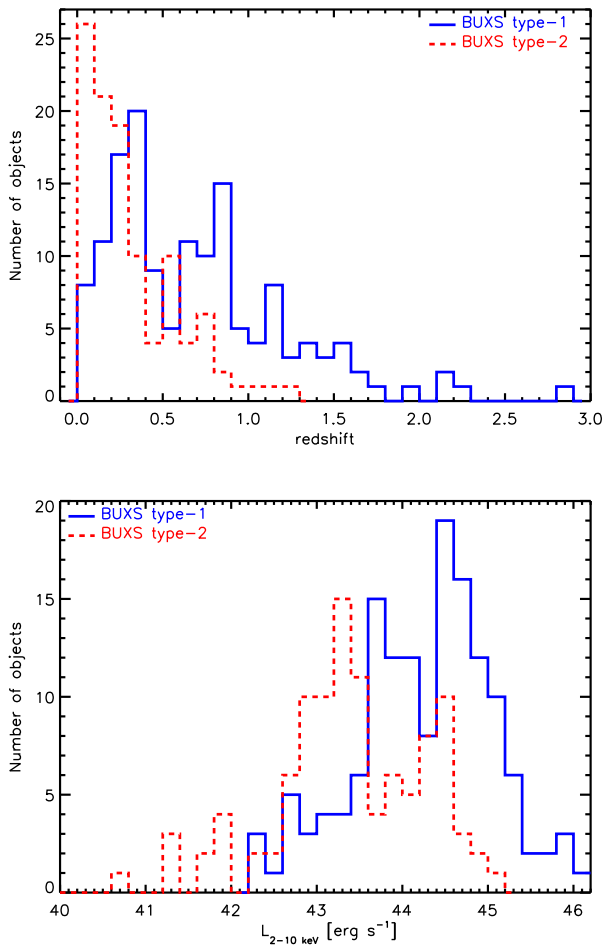


Figure 1. Redshift (top) and 2-10 keV luminosity (in log units, bottom) distributions of the BUXS type-1 and type-2 AGN. Luminosities are rest-frame and are corrected for intrinsic absorption.

et al. 2010). Throughout this paper we use monochromatic MIR flux densities (f_ν) in Janskys, unless otherwise specified.

3 THE BRIGHT ULTRA-HARD *XMM-Newton* SURVEY

BUXS is one of the largest, amongst the existing *XMM-Newton* and *Chandra* surveys, complete flux-limited samples of bright ($f_{4.5-10\text{ keV}} > 6 \times 10^{-14} \text{ erg s}^{-1} \text{ cm}^{-2}$) “ultra-hard” (4.5-10 keV) X-ray selected sources to date. BUXS is based on a subset of 381 high Galactic latitude ($|b| > 20 \text{ deg}$) observations from the second *XMM-Newton* serendipitous source catalogue (2XMM; Watson et al. 2009). The sample is drawn from EPIC-pn observations with clean exposure times $> 10 \text{ ks}$ and having good quality for serendipitous source detection (i.e. free of bright and/or extended X-ray sources). These observations were used to derive extragalactic source count distributions at intermediate fluxes, and therefore we have a good knowledge of the survey completeness (Mateos et al. 2008). The total sky area of BUXS is 44.43 deg^2 .

The selection of sources in the 4.5-10 keV energy band

was motivated by the need to reduce the strong bias against heavily absorbed AGN affecting surveys conducted at softer energies. The BUXS bright flux limit was intended to include only objects for which a reliable classification and redshift could be derived from optical spectroscopy. This also ensures that we can derive accurate X-ray properties such as absorption and intrinsic luminosities from high-quality X-ray spectra ($> \text{few hundred counts}$). In this way we remove uncertainties associated with photometric redshifts and poor X-ray data quality ($< \text{a hundred counts}$). BUXS contains 258 sources after removal of Galactic stars ($< 2\%$) and known BL Lacs ($\sim 1\%$). Optical spectroscopic identifications have been obtained from the Sloan Digital Sky Survey (Abazajian 2009), the literature, and our ongoing follow-up campaign. At the time of writing, the spectroscopic identification completeness is 97.3%. Of the 258 BUXS sources, 145 objects (56.2%) are identified as type-1 AGN (UV/optical emission line velocity widths $\geq 1500 \text{ km s}^{-1}$) and 106 (41.1%) as type-2 AGN (UV/optical emission line velocity widths $< 1500 \text{ km s}^{-1}$ or no emission lines). Seven sources (2.7%) remain unidentified. BUXS covers four decades in X-ray luminosity ($\sim 10^{42} - 10^{46} \text{ erg s}^{-1}$), where the luminosities are computed in the ‘standard’ 2-10 keV rest-frame energy band and are corrected for intrinsic absorption. BUXS identifies sources out to $z \sim 2$. Type-1 and type-2 AGN have mean 2-10 keV luminosities of $1.5 \times 10^{44} \text{ erg s}^{-1}$ and $2.2 \times 10^{43} \text{ erg s}^{-1}$, and mean redshifts of 0.7 and 0.3, respectively. Redshift and luminosity distributions are shown in Fig. 1. We note that BUXS samples absorbed AGN in the Compton-thin regime (rest-frame intrinsic absorption $N_{\text{H}} \lesssim 10^{24} \text{ cm}^{-2}$).

To find the MIR counterparts of the sources in BUXS we used the cross-matching algorithm of Pineau et al. (2011). The algorithm, which is based on the classical likelihood ratio, computes the probability of a spatial coincidence of the X-ray sources with their MIR candidate counterparts. MIR counterparts were found for 255 out of 258 (98.8%) sources (detection with $\text{SNR} \geq 5$ in at least one of the WISE bands). The mean X-ray–MIR separation is $\lesssim 2 \text{ arcsec}$. The three objects without detection in the MIR are type-1 AGN with $z \sim 0.6-0.8$. For one of these sources a blend of two WISE objects prevents us from identifying a unique MIR counterpart. For the other two sources, the expected MIR fluxes, from analysis of their optical/near-IR SEDs, suggest that they are too faint to be detected with WISE.

In order to assess the completeness of our MIR selection technique with respect to the overall AGN population we built a clean AGN parent sample by extracting all catalogued WISE sources in the BUXS survey area, and we identified the objects detected in the 2-10 keV band again using the cross-matching algorithm of Pineau et al. (2011). Here we assume that a detection in hard X-rays is a good tracer of unabsorbed and mildly absorbed AGN activity. We used the 2-10 keV source lists from Mateos et al. (2008) that were derived with the source detection pipeline used in the 2XMM catalogue. The total number of objects in the BUXS area detected in the 2-10 keV X-ray band is 10265. The faintest sources have 2-10 keV fluxes of $\sim 5 \times 10^{-15} \text{ erg s}^{-1} \text{ cm}^{-2}$.

We estimate a fraction of spurious matches of X-ray and MIR sources of $< 1\%$ from the cross-matching of X-ray and WISE sources using a large offset in MIR coordinates (3 arcmin in either RA or dec).

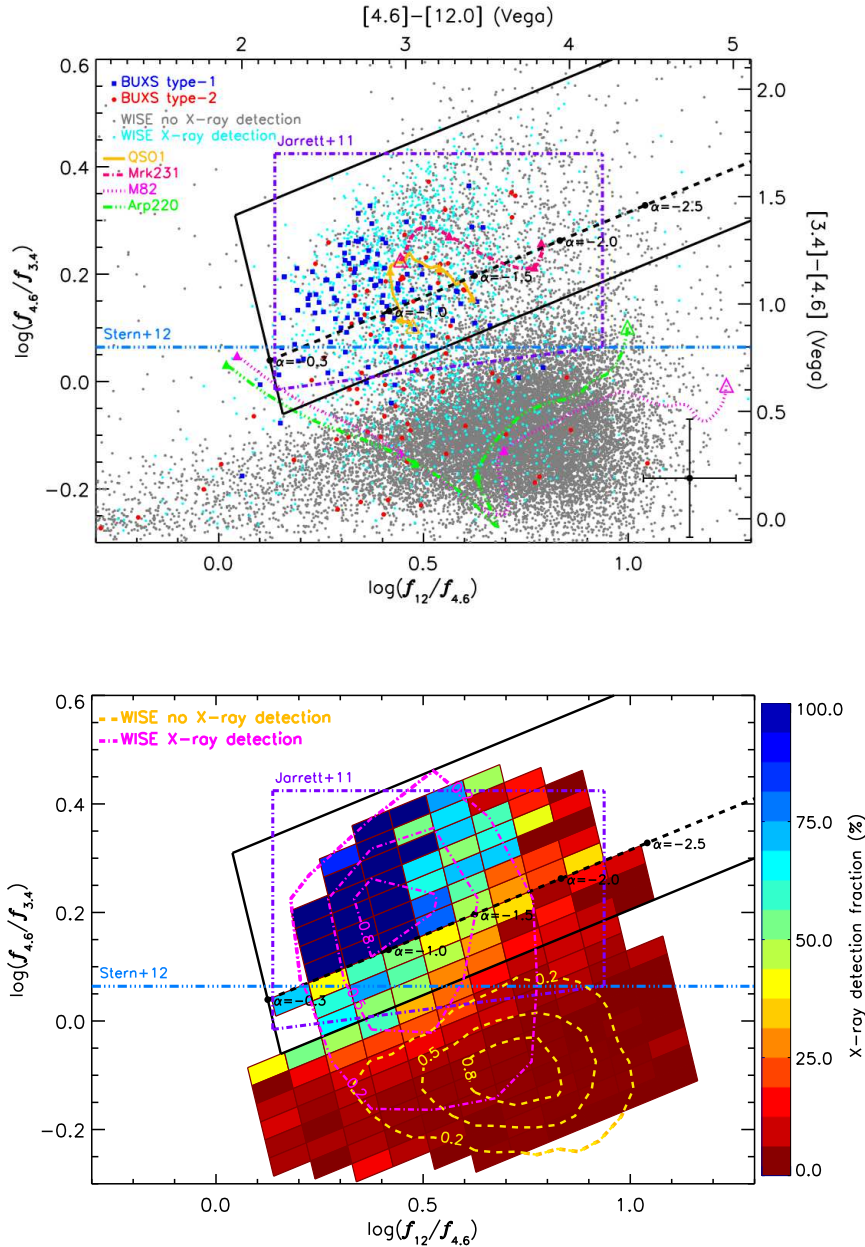


Figure 2. Top: MIR colours for sources detected with $\text{SNR} \geq 5$ at 3.4, 4.6, and 12 μm . Large symbols represent spectroscopically identified BUXS AGN. Small cyan and grey symbols are WISE sources in the BUXS survey area with and without an X-ray detection at 2–10 keV, respectively. The $0 < z \leq 1.5$ ($\Delta z = 0.5$) star-forming tracks represent M82 and the ULIRG Arp220. The $0 < z \leq 3$ ($\Delta z = 0.5$) AGN tracks represent the infrared luminous AGN Mrk231 (Polletta et al. 2008) and a QSO1 template obtained by stitching together the 0.58–3.5 μm near-infrared and 3.5–24 μm MIR quasar composite spectrum from Glikman et al. (2006) and Hernán-Caballero & Hatziminaoglou (2011). Open symbols indicate $z=0$. Our AGN selection wedge and power-law locus are the thick solid and dashed black lines, respectively. For comparison we show the AGN criteria defined by Jarrett et al. (2011) and Stern et al. (2012), respectively (dotted-dashed purple and light blue lines). The error bars show the typical uncertainties in MIR colours at the $\text{SNR}=5$ limit (see Sec. 4.1 for details). Bottom: X-ray detection fraction of WISE objects across the colour-colour plane for bins containing at least 10 sources. Dotted-dashed (magenta) and dashed (yellow) contours indicate the density of WISE sources (normalized to the peak value) with and without X-ray detection, respectively.

4 WISE SELECTION OF AGN CANDIDATES IN THE BUXS FIELDS

(3.4, 4.6, and 12 μm in Sec. 4.1; 3.4, 4.6, 12, and 22 μm in Sec. 4.2).

To avoid spurious detections and objects with poorly constrained photometry, in what follows we restrict ourselves to WISE sources detected with $\text{SNR} \geq 5$ in all relevant bands

Table 1. Summary of the MIR selection of AGN candidates in the BUXS survey area.

MIR wedge (1)	N _{WISE} (2)	N _{WISE+X} (3)	N _{wedge} (4)	N _{wedge+X} (5)
3-band	25206	1659 (6.6%)	2755	1062 (38.5%)
4-band	2476	409 (16.5%)	516	245 (47.5%)

Column 1: MIR AGN selection wedge identifier; Column 2: number of catalogued WISE sources in the BUXS survey area with significance of detection ≥ 5 in the relevant bands; Column 3: number (fraction) of WISE sources with an X-ray detection in the 2-10 keV band; Column 4: number of WISE sources in AGN wedge; Column 5: number (fraction) of WISE sources in AGN wedge and detected in X-rays.

Table 2. Summary of the MIR selection of BUXS AGN.

MIR wedge (1)	Opt. class (2)	N _{WISE} (3)	N _{wedge} (4)
3-band	Type-1	114	105
	Type-2	81	38
	No ID	4	3
4-band	Type-1	63	55
	Type-2	55	21
	No ID	2	1

Column 1: MIR AGN selection wedge identifier; Column 2: Optical class; Column 3: number of sources that are used to define the AGN wedge; Column 4: number of objects in AGN wedge.

4.1 WISE three-band AGN wedge

In the BUXS survey area there are 25206 sources detected with $\text{SNR} \geq 5$ in the three shorter wavelength bands of WISE, of which 1659 have X-ray detections (see Table 1). Out of the latter, 114 are associated with BUXS type-1 AGN and 81 with BUXS type-2 AGN (see Table 2). Fig. 2 shows the MIR $\log(f_{4.6}/f_{3.4})$ vs. $\log(f_{12}/f_{4.6})$ diagram for WISE objects with and without an X-ray counterpart as small cyan and grey symbols, respectively. We also marked with large blue and red symbols spectroscopically classified type-1 and type-2 AGN in the BUXS survey. The dashed line illustrates the MIR power-law locus and the values for different spectral indices. Most BUXS objects, especially type-1 AGN, are clustered near the power-law locus, in a region in the MIR colour-colour plane well separated from the stellar locus (colours near zero magnitude) and the horizontal sequence of normal galaxies (lower right part of the diagram). Furthermore, AGN have, on average, redder $\log(f_{4.6}/f_{3.4})$ colours than a pure power-law. This suggests some curvature in the observed $3.4\mu\text{m}$ to $12\mu\text{m}$ SEDs (e.g. Elvis et al. 1994; Richards et al. 2006; Assef et al. 2010).

Fig. 2 (bottom) shows the fraction of WISE sources detected in X-rays across the colour-colour diagram and the distribution of objects with and without detection in X-rays (contours). There is a clear separation between these distributions. The bulk of the MIR population not detected in X-rays overlaps with the horizontal sequence of normal

galaxies, while the great majority of X-ray detected objects cluster near the power-law locus.

Our MIR-based AGN selection technique is designed to identify objects with red MIR power-law SEDs. The AGN wedge is defined to include all objects with MIR colours expected for power-law SEDs with spectral index $\alpha \leq -0.3$, properly accounting for the typical errors in the photometry at the faintest MIR fluxes (error bars in Fig. 2, top). We then increase the size of the wedge towards red $\log(f_{4.6}/f_{3.4})$ colours (upper boundary) to include all BUXS AGN and the X-ray detected WISE objects throughout the BUXS survey area with such colours. In this way we account for deviations of the $3.4\mu\text{m}$ to $12\mu\text{m}$ SEDs from a pure power-law. Our three-band AGN wedge is shown with the thick solid box in Fig. 2. The MIR power-law locus is defined by

$$y = 0.315 \times x \quad (1)$$

where $x \equiv \log_{10} \left(\frac{f_{12\mu\text{m}}}{f_{4.6\mu\text{m}}} \right)$ and $y \equiv \log_{10} \left(\frac{f_{4.6\mu\text{m}}}{f_{3.4\mu\text{m}}} \right)$. The top and bottom boundaries of the wedge are obtained by adding y-axis intercepts of +0.297 and -0.110, respectively. The MIR power-law $\alpha = -0.3$ bottom-left limit corresponds to

$$y = -3.172 \times x + 0.436 \quad (2)$$

These are the limits we have used throughout this paper. However, for most practical purposes using instead a bottom-left vertical limit, corresponding to $x \geq 0.120$, produces very similar results.

In Vega magnitudes (in the WISE source catalogue magnitudes are reported in the Vega system), the AGN locus is defined by

$$y' = 0.315 \times x' \quad (3)$$

where $x' \equiv [4.6] - [12]$ and $y' \equiv [3.4] - [4.6]$. The top and bottom boundaries of the wedge are obtained by adding y-axis intercepts of +0.796 and -0.222, respectively. In this case, the MIR power-law $\alpha = -0.3$ bottom-left limit corresponds to

$$y' = -3.172 \times x' + 7.624 \quad (4)$$

The bottom-left vertical limit of the AGN wedge in magnitudes corresponds to $x' \geq 2.157$.

Our three-band AGN wedge identifies 2755 AGN candidates in the BUXS area, of which 1062 (38.5%) are detected in X-rays (see Table 1). Out of the latter, 105 are associated with BUXS type-1 AGN and 38 with BUXS type-2 AGN (see Table 2). We note that the X-ray detection fraction in the wedge increases with the depth of the X-ray observations as shown in Table 3. For example, in the BUXS area where the X-ray observations have exposures > 40 ks, the X-ray detection fraction rises to 49.8%. For comparison, in the 1Ms CDF-S survey the X-ray detection fraction of IRAC power-law AGN candidates was $\sim 50\%$ (Alonso-Herrero et al. 2006) while this fraction increased to $\sim 85\%$ in the deeper 2Ms CDF-N survey (Donley et al. 2007). Furthermore, Donley et al. (2012) found that the X-ray detection fraction of IRAC MIR AGN candidates in COSMOS increased from 38% to 52% in the regions of deep *Chandra* coverage (X-ray exposures 50-160 ks). This is as expected, as long X-ray exposures are required to detect intrinsically less luminous and/or heavily obscured AGN (see e.g. Mateos et al. 2005; Tozzi et al.

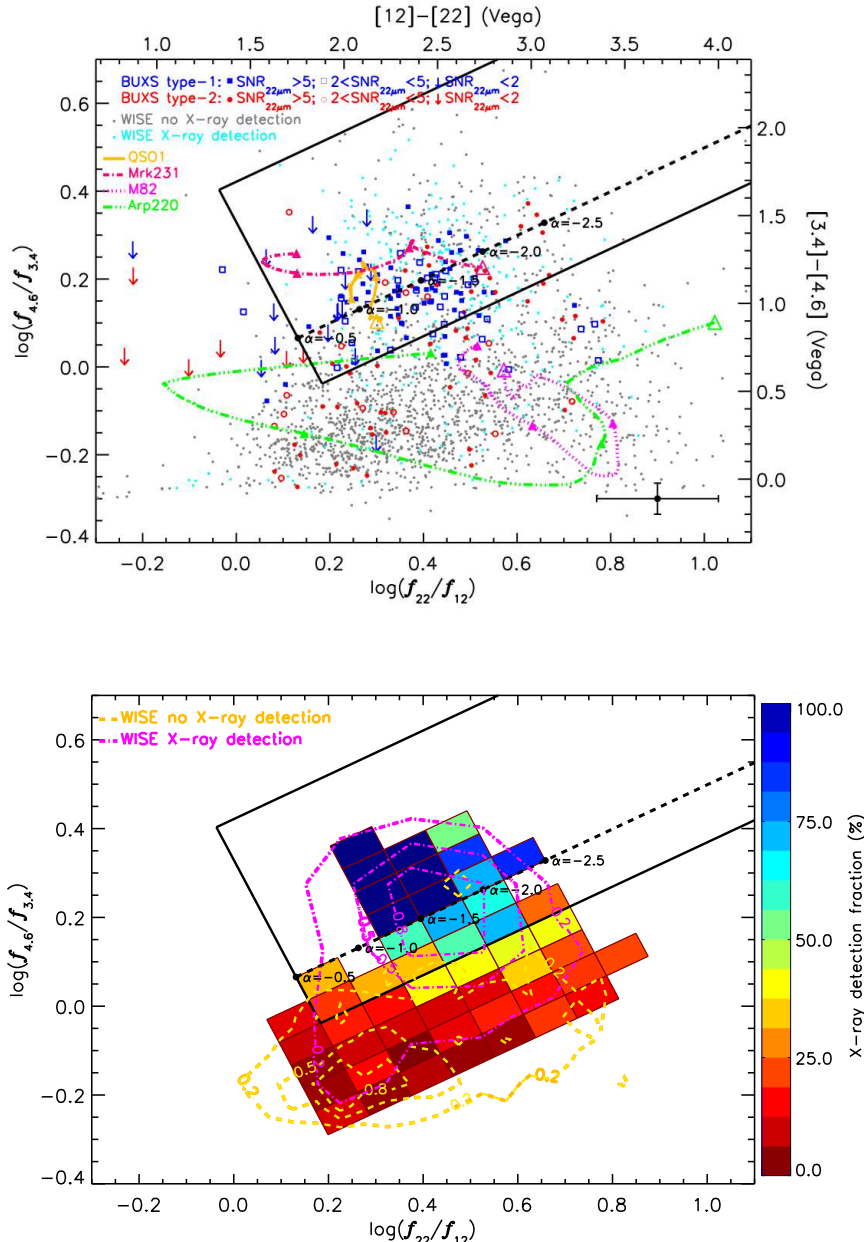


Figure 3. Equivalent to Fig. 2 for a MIR-based AGN selection using the complete four bands of WISE. Top: We include all objects with $\text{SNR} \geq 5$ at 3.4, 4.6, and $12\mu\text{m}$ and use different symbols depending on the $22\mu\text{m}$ significance of detection. For $\text{SNR} < 2$ at $22\mu\text{m}$ we use 1σ fluxes as upper limits. Symbols as in Fig. 2.

2006; Comastri et al. 2011; Brightman et al. 2012). Still, a substantial fraction of our MIR AGN candidates are undetected at 2-10 keV energies with the typical exposures in the 2XMM catalogue. These objects that have the reddest overall $\log(f_{12}/f_{4.6})$ colours in the AGN wedge, are the best candidates to account for the most heavily obscured/absorbed luminous AGN missed by hard X-ray surveys. Lacy et al. (2007) presented the optical spectroscopic followup of a sample of luminous AGN candidates selected on the basis of their IRAC MIR colours. They confirmed the AGN nature of 91% of the sources, with the majority of the objects being identified as dust-reddened type-1 quasars and type-2 AGN. Furthermore, a detailed study of the WISE MIR SEDs

of [OIII]5007Å-selected QSO2s (Reyes et al. 2008) strongly supports our hypothesis that many of the X-ray undetected sources in the wedge are heavily-obscured very-luminous AGN (Mateos et al. 2012b, in prep.).

4.2 WISE four-band AGN wedge

Due to the significantly shallower depth at $22\mu\text{m}$ compared with the first three bands, a selection that uses the $22\mu\text{m}$ survey will be restricted by necessity to the brightest MIR objects. We have investigated, however, whether we can gain any additional information on AGN selection by using the complete four WISE bands. The number of MIR sources de-

Table 3. Dependence of the X-ray detection fraction of WISE sources in the 3-band AGN wedge as a function of the exposure time of the *XMM-Newton* observations.

t_{exp} (1)	N_{wedge} (2)	$N_{\text{wedge+X}}$ (3)
10–20	1225	400 (32.7%)
20–30	723	298 (41.2%)
30–40	347	135 (38.9%)
40–50	210	110 (52.4%)
>50	250	119 (47.6%)
Total	2755	1062 (38.5%)

Column 1: EPIC-pn exposure time interval of the X-ray observations in units of ks; Column 2: number of catalogued WISE sources in AGN wedge with significance of detection ≥ 5 in the three shorter wavelength bands of WISE. Column 3: number (fraction) of WISE sources in AGN wedge with an X-ray detection in the 2–10 keV band.

tected with $\text{SNR} \geq 5$ in all four WISE bands in the area of BUXS is 2476, of which 409 are detected in X-rays. Out of the latter, 63 are associated with BUXS type-1 AGN and 55 with BUXS type-2 AGN (see Tables 1 and 2). Fig. 3 (top) shows the distribution of $\log(f_{4.6}/f_{3.4})$ vs. $\log(f_{22}/f_{12})$ colours. The solid lines illustrate the four-band AGN selection wedge as in Sec. 4.1. In this case we increase the size of the wedge that would be required to account for the typical photometric errors (error bars in Fig. 3) towards both redder $\log(f_{22}/f_{12})$ and $\log(f_{4.6}/f_{3.4})$ colours. In this way we increase the completeness of the selection without compromising the reliability. The MIR power-law locus is defined by

$$y = 0.50 \times x \quad (5)$$

where $x \equiv \log_{10} \left(\frac{f_{22\mu\text{m}}}{f_{12\mu\text{m}}} \right)$ and $y \equiv \log_{10} \left(\frac{f_{4.6\mu\text{m}}}{f_{3.4\mu\text{m}}} \right)$. The top and bottom boundaries of the wedge are obtained by adding y-axis intercepts of +0.421 and -0.130 , respectively. In this case we use a MIR power-law bottom-left limit of $\alpha = -0.5$ that corresponds to

$$y = -2.00 \times x + 0.33 \quad (6)$$

These are the limits we have used in Sec. 4.3. Using instead a bottom-left vertical limit, corresponding to $x \geq 0.13$, produces very similar results.

In Vega magnitudes the AGN locus is defined by

$$y' = 0.50 \times x' \quad (7)$$

where $x' \equiv [12] - [22]$ and $y' \equiv [3.4] - [4.6]$. The top and bottom boundaries of the wedge are obtained by adding y-axis intercepts of +0.979 and -0.405 , respectively. In this case, the MIR power-law $\alpha = -0.5$ bottom-left limit corresponds to

$$y' = -2.00 \times x' + 4.33 \quad (8)$$

The bottom-left vertical limit of the AGN wedge in magnitudes corresponds to $x' \geq 1.76$.

Our four-band AGN wedge identifies 516 AGN candidates in the BUXS area detected with $\text{SNR} \geq 5$ in all four WISE bands, of which 245 (47.5%) are detected in X-rays.

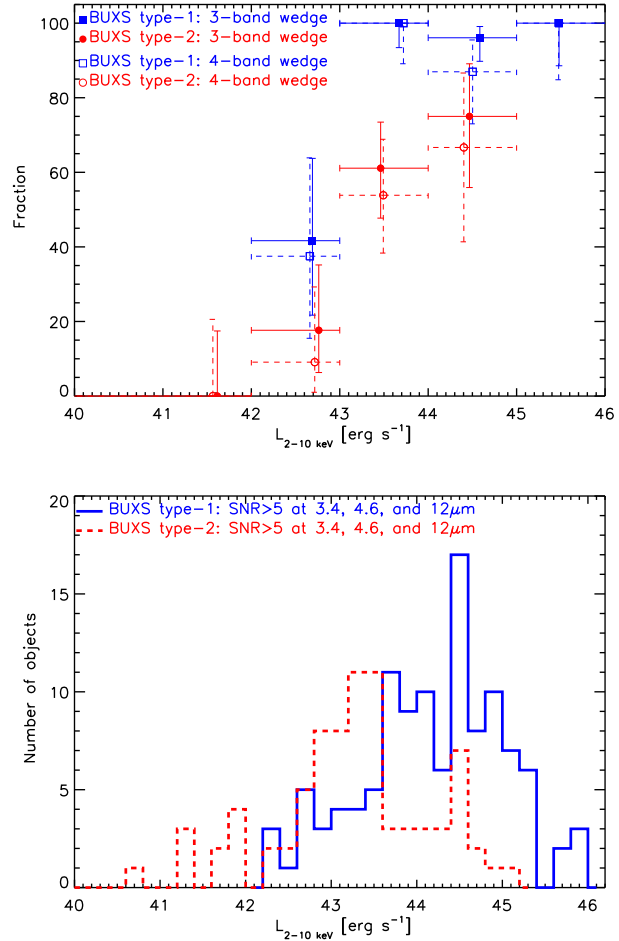


Figure 4. Top: Fraction of BUXS AGN that meet our MIR selection as a function of their intrinsic 2–10 keV luminosity (in log units). Filled symbols show selection using the three shorter wavelength bands of WISE and open symbols show selection using the complete four bands. The symbols indicate the mean luminosity of the sources in the bin. Bottom: Distributions of 2–10 keV luminosity (in log units) for the BUXS type-1 and type-2 AGN detected with $\text{SNR} \geq 5$ in the three shorter wavelength bands of WISE. The luminosity (and redshift) distributions of the BUXS AGN detected in the three shorter wavelength bands of WISE and the complete four bands are consistent with each other.

Out of the latter, 55 are associated with BUXS type-1 AGN and 21 with BUXS type-2 AGN (see Table 2).

4.3 AGN selection completeness

Fig. 4 (top) and Table 4 show the fraction of BUXS AGN that meet our three-band MIR colour cuts as a function of their intrinsic 2–10 keV luminosity (filled symbols). The symbols indicate the mean luminosity of the sources in the bin. Rest-frame luminosities were derived from a detailed X-ray spectroscopic analysis and are corrected for Galactic and any intrinsic absorption. The completeness of our selection criteria is a strong function of luminosity for both type-1 and type-2 AGN. This result reflects the fact that objects with MIR colours not dominated by the thermal emission from the AGN will be missed by our selection. This effect is more im-

portant for low-luminosity AGN, especially if these sources are affected by large dust extinction at the shortest wavelengths of WISE. In these objects the starlight from the host galaxy will dominate their MIR emission. Thus, it should be emphasized that the comparison of an MIR colour selection completeness for different classes of objects is only meaningful if the objects span the same range of luminosities. Taking this into account, at $L_{2-10\text{ keV}} < 10^{44}\text{erg s}^{-1}$, $84.4^{+7.4}_{-10.0}\%$ and $39.1^{+10.1}_{-9.5}\%$ of the type-1 and type-2 AGN, respectively meet the selection. At $L_{2-10\text{ keV}} \geq 10^{44}\text{erg s}^{-1}$ the MIR selection efficiency increases to $97.1^{+2.2}_{-4.8}\%$ and $76.5^{+13.3}_{-18.4}\%$ for type-1 and type-2 AGN, respectively. We estimated the most probable value for these fractions using a Bayesian approach and the binomial distribution from Wall & Jenkins (2008). The quoted errors are the narrowest interval that includes the mode and encompasses 90% of the probability (S. Andreon, private communication). It is important to note that the significantly smaller value of the selection completeness obtained for type-2 AGN at $L_{2-10\text{ keV}} < 10^{44}\text{erg s}^{-1}$ compared to that for type-1 AGN is mainly due, as indicated above, to the different luminosity distributions of the two classes of AGN. The type-2 AGN population in BUXS is dominated by objects with $L_{2-10\text{ keV}} \lesssim 10^{44}\text{erg s}^{-1}$ ($\sim 79\%$ vs. $\sim 39\%$ for type-1 AGN; see Fig. 4 bottom). At such luminosities many AGN have relatively blue colours at the shortest WISE wavelengths (i.e. host-dominated) and thus lie outside the MIR AGN wedge. We expect this effect to be more important for type-2 AGN, as this class of objects is expected to show a higher degree of extinction at the shortest wavelengths of WISE. For example, the clumpy torus models of Nenkova et al. (2008) predict nearly isotropic emission at wavelengths $\gtrsim 12\mu\text{m}$. This could explain that even if we use the same luminosity range (as in Fig. 4) we obtain a selection completeness that is, within the uncertainties, still marginally lower for type-2 AGN than for type-1 AGN. This result still holds at luminosities $L_{2-10\text{ keV}} > 10^{44}\text{erg s}^{-1}$, where the relative contribution of the host galaxy to the MIR emission should be small. However, as the number of type-2 AGN in BUXS at such luminosities is small (16 objects), the difference could be due in part to small number statistics. Thus, we conclude that our 3-band AGN wedge is highly complete for both X-ray selected luminous type-1 and type-2 AGN.

Fig. 4 (top) and Table 5 show the fraction of BUXS AGN that meet our four-band colour cuts as a function of their intrinsic 2-10 keV luminosity (open symbols). The completeness of the four-band wedge is somewhat smaller but comparable, within the uncertainties, to that achieved with the three-band selection for both type-1 and type-2 AGN. Indeed, 76 out of the 118 BUXS AGN detected in the four WISE bands meet the four-band selection, while this number increases to 88 if the three-band selection is used instead. All the 15 three-band selected BUXS AGN that miss the four-band selection have $\log(f_{22}/f_{12})$ colours significantly redder than those expected for a pure power-law SED. These objects lie outside the four-band AGN wedge, in the region of the colour-colour plane occupied by normal star-forming galaxies. They likely miss the four-band selection because their $22\mu\text{m}$ emission comes from both AGN activity and intense star formation. On the other hand, only three BUXS AGN from the four-band selection lie outside the three-band wedge. We note that we obtain the same result if we in-

Table 4. Dependence of the WISE 3-band AGN wedge completeness on the luminosity of the BUXS AGN.

$\log(L_{2-10\text{ keV}})$ (1)	$N_{\text{type-1}}$ (2)	$f_{\text{type-1}}$ (3)	$N_{\text{type-2}}$ (4)	$f_{\text{type-2}}$ (5)
[40–42]	-	-	11	$0.0^{+17.4}$
[42–43]	12	$41.7^{+22.1}_{-20.0}$	17	$17.6^{+17.5}_{-11.3}$
[43–44]	33	$100^{+6.6}_{-6.6}$	36	$61.1^{+12.3}_{-13.4}$
[44–45]	51	$96.1^{+3.0}_{-6.3}$	16	$75.0^{+14.1}_{-19.1}$
[45–46]	18	$100^{+11.4}_{-11.4}$	1	-
Total	114		81	

Column 1: X-ray luminosity range in units of erg s^{-1} (logarithmic units, 2-10 keV in rest-frame and corrected for any intrinsic absorption); Column 2: number of BUXS type-1 AGN in luminosity bin; Column 3: fraction of BUXS type-1 AGN in the WISE 3-band AGN wedge; Column 4: number of BUXS type-2 AGN in luminosity bin; Column 5: fraction of BUXS type-2 AGN in the WISE 3-band AGN wedge.

Table 5. Dependence of the WISE 4-band AGN wedge completeness on the luminosity of the BUXS AGN.

$\log(L_{2-10\text{ keV}})$ (1)	$N_{\text{type-1}}$ (2)	$f_{\text{type-1}}$ (3)	$N_{\text{type-2}}$ (4)	$f_{\text{type-2}}$ (5)
[40–42]	-	-	9	$0.0^{+20.6}$
[42–43]	8	$37.5^{+26.4}_{-22.0}$	11	$9.1^{+20.2}_{-8.1}$
[43–44]	19	$100^{+10.9}_{-10.9}$	26	$53.8^{+15.0}_{-15.5}$
[44–45]	23	$87.0^{+8.5}_{-14.0}$	9	$66.7^{+20.0}_{-25.3}$
[45–46]	13	$100^{+15.2}_{-15.2}$	-	-
Total	63		55	

Column 1: X-ray luminosity range in units of erg s^{-1} (logarithmic units, 2-10 keV in rest-frame and corrected for any intrinsic absorption); Column 2: number of BUXS type-1 AGN in luminosity bin; Column 3: fraction of BUXS type-1 AGN in the WISE 4-band AGN wedge; Column 4: number of BUXS type-2 AGN in luminosity bin; Column 5: fraction of BUXS type-2 AGN in the WISE 4-band AGN wedge.

clude all BUXS AGN with a lower significance of detection at $22\mu\text{m}$ (open symbols and arrows in Fig. 3, top). Therefore, by requiring $22\mu\text{m}$ detections we are not biased against AGN with pure power-law SEDs (i.e. the faintest objects at $22\mu\text{m}$). Thus, by including the $22\mu\text{m}$ WISE band to select AGN candidates neither the completeness nor the reliability of the selection improves.

We have checked that using non-contiguous bands to define the WISE MIR colours does not increase the completeness of a three-band or a four-band selection.

5 RELIABILITY OF THE THREE-BAND AGN WEDGE

In the following we restrict ourselves to the three-band AGN wedge which, as shown in the previous section, provides the most complete selection of AGN candidates in the BUXS fields with WISE.

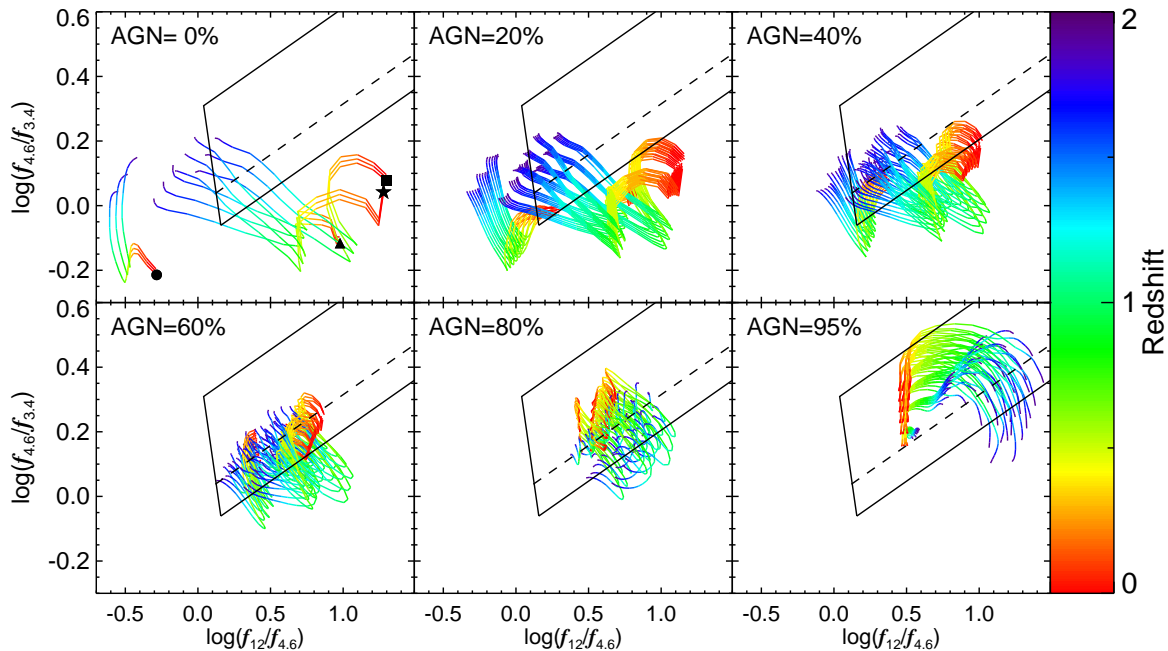


Figure 5. Predicted $z=0-2$ WISE colours of AGN/galaxy composite SEDs for our three-band AGN wedge. The AGN fraction is defined between 1 and 10 μm . The star-forming templates represent the ULIRG IRAS 22491 (square, Polletta et al. 2008), the starburst M82 (star, Polletta et al. 2008), a normal star-forming spiral galaxy (triangle, Dale et al. 2002), and an elliptical galaxy (circle, Polletta et al. 2008). Large symbols mark each family of purely star-forming templates at $z=0$. The AGN template is the QSO1 template of Polletta et al. (2008). Additional extinctions of $A_V = 0 - 2$ and $A_V = 0 - 20$ are applied to the star-forming and AGN components, respectively. Our MIR AGN selection wedge and power-law locus are the thick solid and dashed black lines, respectively. The power-law locus is defined from $\alpha = -0.3$. The colour tracks of purely star-forming galaxies would enter our selection wedge at $z \gtrsim 1.3$. At such redshifts however, most galaxies are too faint to be detected at the relatively shallow $12\mu\text{m}$ flux density limits.

5.1 Comparison with templates

A known limitation of MIR selection techniques is the contamination from galaxies without AGN activity where the major contributor to the MIR emission is the stellar population or strong star formation (e.g. Lacy et al. 2004; Stern et al. 2005; Jarrett et al. 2011; Donley et al. 2012; Stern et al. 2012). To assess the reliability of our three-band AGN wedge we show in Fig. 5 the expected WISE colours of AGN with varying host-galaxy contributions following Donley et al. (2012). The composite SEDs were constructed using the library of Polletta et al. (2008) and the normal star-forming spiral galaxy template from Dale et al. (2002). The solid and dashed lines illustrate the AGN wedge along with the power-law locus, respectively. We also applied additional extinctions of $A_V=0-2$ and $A_V=0-20$ to the star-forming and AGN components, respectively, using the Draine et al. (2003) extinction curve. The colour tracks of pure star-forming galaxies would enter our selection wedge at $z \gtrsim 1.3$. At such redshifts, however, most galaxies are too faint to be detected at the relatively shallow WISE flux density limits (Wright et al. 2010; Jarrett et al. 2011). Indeed, in the region of the AGN wedge where we would expect contamination from normal star-forming galaxies, there is no clear excess of MIR X-ray undetected sources and the X-ray detection fraction remains high (see Fig. 2). Thus it seems that at the adopted $\text{SNR} \geq 5$ limit our AGN selection suffers

from minimal contamination from high redshift pure star-forming galaxies. It is interesting to note that an important fraction of the X-ray detected WISE sources has $\log(f_{12}/f_{4.6})$ colours bluer than those expected for a pure AGN SED. The WISE colour tracks of composite galaxies suggest that this is most likely due to both AGN and their host galaxies contributing to the observed emission in the WISE bands. On the other hand, we find a sharp decrease in the X-ray detection fraction of WISE objects at $\log(f_{12}/f_{4.6}) \gtrsim 0.7-0.8$. At such red MIR colours we expect many objects to be heavily obscured AGN. However, the colour tracks of pure AGN indicate that there is a strong dependence of the observed $\log(f_{12}/f_{4.6})$ colour with redshift. This suggests that the population of WISE objects with $\log(f_{12}/f_{4.6}) \gtrsim 0.7-0.8$ could be a mixture of heavily absorbed AGN and objects at high redshifts ($z \gtrsim 1-1.5$).

5.2 Comparison with other WISE selection techniques

Within the BUXS survey area our three-band MIR colour selection identifies 2755 AGN candidates, of which 1062 sources (38.5%) are detected in X-rays. For comparison, the X-ray detection fraction of WISE objects that meet the Jarrett et al. (2011) colour-based AGN selection (indicated in Fig. 2) is 33.4% (see Table 6). At red MIR colours their

Table 6. Comparison of our AGN wedge with other WISE selection techniques.

MIR wedge (1)	N_{wedge} (2)	$N_{\text{wedge}+X}$ (3)
Mateos 3-band	2755	1062 (38.5%)
Jarrett+11	3301	1102 (33.4%)
Stern+12	3946	1254 (31.8%)

Column 1: MIR AGN selection criteria; Column 2: number of catalogued WISE AGN candidates in the BUXS survey area. For the Jarrett et al. (2011) wedge we selected only MIR objects with significance of detection ≥ 5 in the three shorter wavelength bands of WISE as in our analysis. The Stern et al. (2012) selection only requires an MIR detection at $4.6\mu\text{m}$, brighter than $160\mu\text{Jy}$ (see Sec. 5.2 for details). Column 3: number (fraction) of WISE sources in AGN wedge with an X-ray detection in the 2-10 keV band.

selection enters the sequence of low redshift normal galaxies increasing the expected number of contaminants.

Stern et al. (2012) proposed an AGN selection using a $[3.4]-[4.6]$ colour cut ($[3.4]-[4.6] \geq 0.8$ or $\log(f_{4.6}/f_{3.4}) \geq 0.06$) and a $4.6\mu\text{m}$ flux threshold of $160\mu\text{Jy}$. Their argument was that the inclusion of the longer wavelength WISE data would increase the reliability of the AGN selection but at the cost of reducing the completeness. Fig. 2 and Fig. 5 show that the $[3.4]-[4.6]$ colour cut proposed by Stern et al. (2012) also enters the locus of low redshift normal galaxies at red $\log(f_{12}/f_{4.6})$ colours. This could reduce the reliability of their selection as suggested by the lower X-ray detection fraction of WISE sources in the BUXS area that meet their criteria (31.8%; see Table 6). On the other hand, using the deep (60-160 ks) *Chandra* data available in the COSMOS field, Stern et al. (2012) find that 87% of their WISE AGN candidates are detected at X-ray energies, suggesting minimal contamination from normal galaxies.

The *XMM-Newton* pointings used to build BUXS span a broad range of ecliptic latitudes and thus the depth of the WISE survey varies across the BUXS fields. The Stern et al. (2012) AGN selection was defined using the COSMOS field located at low ecliptic latitude and thus, the MIR data are close to the minimum depth of the WISE survey. At such shallow depths and using the Stern et al. (2012) $160\mu\text{Jy}$ flux threshold at $4.6\mu\text{m}$, many of the star-forming contaminants will be too faint to be detected, thereby increasing the reliability of the Stern et al. (2012) selection. Although BUXS likely samples fainter objects than those best targeted at the shallow depth of WISE, we find that $\sim 98\%$ of the AGN have MIR detections with $\text{SNR} \geq 5$ at $3.4\mu\text{m}$ and $4.6\mu\text{m}$. This fraction only decreases to $\sim 77\%$ if we require $12\mu\text{m}$ detections with $\text{SNR} \geq 5$. In conclusion, over the range of MIR depths of the WISE survey in the BUXS fields, our proposed selection suffers less contamination from star-forming galaxies than provided by a simple $[3.4]-[4.6]$ color cut, while only marginally reducing completeness.

We have investigated the impact of increasing the MIR significance of detection of the AGN candidates. If we require $3.4\mu\text{m}$ and $4.6\mu\text{m}$ detections with $\text{SNR} \geq 10$, 44% of our MIR AGN candidates with $\log(f_{12}/f_{4.6}) \geq 0.6$ will be missed (21% of the objects with an X-ray detection), while this frac-

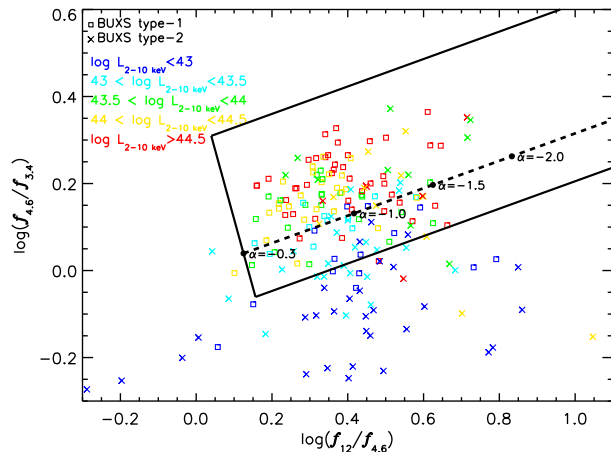


Figure 6. MIR colours of BUXS AGN as a function of intrinsic 2-10 keV luminosity. Solid and dashed lines illustrate the AGN selection wedge and power-law locus, respectively. Most BUXS type-2 AGN are objects with $L_{2-10\text{ keV}} \lesssim 10^{44}\text{ergs}^{-1}$ ($\sim 79\%$ vs. $\sim 39\%$ for type-1 AGN; see Fig. 4). At such luminosities many AGN have relatively blue colours at the shortest WISE wavelengths (i.e., host-dominated) and lie outside the AGN wedge.

tion is only 0.7% at $\log(f_{12}/f_{4.6}) \leq 0.6$ (and zero for objects with an X-ray detection). Therefore, the effect of increasing the threshold in SNR of the detections is that the resulting MIR selection becomes increasingly similar to a hard X-ray selection. By using $\text{SNR} \geq 5$ WISE sources, we gain in the identification of AGN candidates with the reddest MIR colours, while we do not reduce the reliability.

It is clear that our MIR colour selection is a good compromise between completeness and the crucial high reliability required to obtain a clean sample of powerful AGN at the different depths of the WISE survey. Furthermore, going down to detections with $\text{SNR} \geq 5$, we reach a much higher efficiency of detection of the AGN population in the reddest MIR colours, many of which could be heavily obscured/extincted AGN.

5.3 Trends in the wedge with the AGN luminosity

In the previous sections we presented the WISE expected colours for AGN/star-forming galaxies derived from a library of templates. Here we investigate in more detail the colour trends in the three-band AGN wedge for the BUXS type-1 and type-2 AGN. Fig. 6 shows the MIR colours of the AGN in BUXS as a function of their X-ray luminosity. As expected, there is a strong dependence of $\log(f_{4.6}/f_{3.4})$ on the X-ray luminosity, with less luminous sources having the bluest MIR colours. For less powerful AGN the host galaxy can substantially contribute to the MIR emission (e.g. Buchanan et al. 2006; Alonso-Herrero et al. 2008). Host galaxy dilution is expected to be more important in type-2 AGN, especially at low luminosities, as type-2 AGN should show a higher degree of extinction at the shortest wavelengths of WISE. These objects, with MIR colours consistent with normal galaxies, lie outside of the AGN wedge and thus, they are missed from a pure MIR selection. Fig. 2 and Fig. 6 both show that most AGN in BUXS missed by

the 3-band wedge are type-2 AGN. As noted in Sec. 4.3, in flux-limited X-ray surveys, such as BUXS, type-2 AGN are overall intrinsically less luminous than type-1 AGN (see Fig. 1, bottom). Thus, due to the strong dependence of the MIR selection completeness on the luminosity of the objects (see Fig. 4, top), our AGN wedge will preferentially pick out BUXS type-1 AGN. However, at luminosities $L_{2-10\text{ keV}} > 10^{44}\text{ erg s}^{-1}$, where the AGN is expected to dominate the MIR emission (unless it is heavily absorbed), the completeness of the selection of type-1 and type-2 AGN is comparable within the uncertainties. At such luminosities both type-1 and type-2 AGN are preferentially located above the power-law locus (see also Fig. 5). This indicates that the observed $3.4\mu\text{m}$ to $12\mu\text{m}$ MIR SEDs of powerful AGN deviate from a pure power-law.

We do not find a strong dependence of the $\log(f_{12}/f_{4.6})$ colour on the X-ray luminosity. However, we find a large scatter in the distribution of $\log(f_{12}/f_{4.6})$ colours, especially for objects at low luminosities, where the host galaxy significantly contributes to the MIR emission. A broad range of $\log(f_{12}/f_{4.6})$ colours is expected for AGN with an important host galaxy contribution as the very wide $12\mu\text{m}$ filter of WISE is very sensitive to both prominent PAH emission features and silicate absorption ($10\mu\text{m}$) in star-forming galaxies over a broad range of redshifts.

6 SUMMARY

We present a MIR power-law based selection of luminous AGN candidates using the 3.4, 4.6, and $12\mu\text{m}$ bands of the WISE survey. We defined an AGN wedge in the $\log(f_{4.6}/f_{3.4})$ vs. $\log(f_{12}/f_{4.6})$ colour-colour diagram using the Bright Ultra-Hard *XMM-Newton* Survey (BUXS). This is one of the largest complete flux-limited samples of bright ($f_{4.5-10\text{ keV}} > 6 \times 10^{-14}\text{ erg s}^{-1}\text{ cm}^{-2}$) “ultra-hard” (4.5-10 keV) X-ray selected AGN to date. BUXS includes 258 objects detected over a total sky area of 44.43 deg^2 : 251 (97.3%) are spectroscopically identified and classified, with 145 being type-1 AGN and 106 type-2 AGN. Our technique is based on a MIR power-law selection and properly accounts for the errors in the photometry and deviations of the MIR spectral energy distributions from a pure power-law. In flux-limited X-ray surveys, such as BUXS, type-2 AGN are intrinsically less luminous than type-1 AGN. Thus, due to the strong dependence of the MIR selection completeness on the luminosity of the objects, a MIR AGN wedge necessarily picks out BUXS type-1 AGN. However, at 2-10 keV luminosities above $10^{44}\text{ erg s}^{-1}$ the completeness of our MIR selection of type-1 and type-2 AGN is high and comparable for both types within the uncertainties. Our selection is highly complete at luminosities $L_{2-10\text{ keV}} > 10^{44}\text{ erg s}^{-1}$ where our MIR wedge recovers $\sim 97\%$ and $\sim 77\%$ of the BUXS type-1 and type-2 AGN, respectively. We identify 2755 AGN candidates in the 44.43 deg^2 BUXS survey area of which 38.5% have detection in X-rays. In the BUXS area where the X-ray observations have exposures $> 40\text{ ks}$, the X-ray detection fraction rises to 49.8%. This is reasonable, as long X-ray exposures are required to detect intrinsically less luminous and/or heavily obscured AGN. A substantial fraction of the MIR AGN candidates remain undetected at 2-10 keV energies with the typical exposures in the

2XMM catalogue. These objects are the best candidates to account for the most heavily obscured/absorbed luminous AGN missed by hard X-ray surveys. Assuming that a 2-10 keV X-ray detection is a good tracer of AGN activity we demonstrate that our WISE selection shows one of the highest reliability amongst those in the literature. This is crucial to obtain a clean MIR selection of powerful AGN. Furthermore, going down to a $\text{SNR} \geq 5$ limit in the WISE flux densities, we substantially increase the efficiency of detection of AGN with the reddest MIR colours. We also investigate a WISE four-band AGN selection. We show, however, that by including the $22\mu\text{m}$ WISE band neither the completeness nor the reliability of the selection improves. This is likely due to both the significantly shallower depth at $22\mu\text{m}$ compared with the first three bands of WISE and star-formation contributing to the $22\mu\text{m}$ emission at the WISE $22\mu\text{m}$ sensitivity.

ACKNOWLEDGMENTS

This work is based on observations obtained with *XMM-Newton*, an ESA science mission with instruments and contributions directly funded by ESA Member States and NASA. Based on data from the Wide-field Infrared Survey Explorer, which is a joint project of the University of California, Los Angeles, and the Jet Propulsion Laboratory/California Institute of Technology, funded by the National Aeronautics and Space Administration. Funding for the SDSS and SDSS-II has been provided by the Alfred P. Sloan Foundation, the Participating Institutions, the National Science Foundation, the U.S. Department of Energy, the National Aeronautics and Space Administration, the Japanese Monbukagakusho, the Max Planck Society, and the Higher Education Funding Council for England. The SDSS Web Site is <http://www.sdss.org/>. Based on observations collected at the European Organisation for Astronomical Research in the Southern Hemisphere, Chile, programme IDs 084.A-0828, 086.A-0612, 087.A-0447. Based on observations made with the William Herschel Telescope -operated by the Isaac Newton Group-, the Telescopio Nazionale Galileo -operated by the Centro Galileo Galilei and the Gran Telescopio de Canarias installed in the Spanish Observatorio del Roque de los Muchachos of the Instituto de Astrofísica de Canarias, in the island of La Palma. SM, FJC and XB acknowledge financial support by the Spanish Ministry of Economy and Competitiveness through grant AYA2010-21490-C02-01. A.A.-H. acknowledges support from the Universidad de Cantabria through the Augusto G. Linares program. A.B. acknowledges a Royal Society Wolfson Research Merit Award. J.L.D. acknowledges support from the LANL Director’s Fellowship. P.S. acknowledges financial support from ASI (grant No. I/009/10/0). The authors wish to thank the anonymous referee for constructive comments.

REFERENCES

- Abazajian, K. N., Adelman-McCarthy, J. K., Agüeros, M. A., et al. 2009, *ApJS*, 182, 543
- Alexander D.M., Bauer F.E., et al. 2011, *ApJ*, 738, 44A

- Alonso-Herrero A., Pérez-González P. G., Alexander D. M., et al. 2006, *ApJ*, 640, 167
- Alonso-Herrero A., Pérez-González P. G., Rieke G.H., et al. 2008, *ApJ*, 677, 127
- Assef R. J., Kochanek C. S., et al. 2010, *ApJ*, 713, 970
- Bird A.J., Malizia A., et al. 2007, *ApJS*, 170, 175
- Brightman M., Ueda Y., et al. 2012, *MNRAS*, 423, 702
- Buchanan C. L., Gallimore J. F., et al. 2006, *AJ*, 132, 401
- Burlon D., Ajello M., Greiner J., et al. 2011, *ApJ*, 728, 58
- Caccianiga A., Severgnini P., et al. 2004, *MNRAS*, 416, 901
- Comastri A., Ranalli P., Iwasawa K., et al. 2011, *A&A*, 526, 9
- Cutri R. M., Wright E. L., Conrow T., et al. 2012, Explanatory Supplement to the WISE All-Sky Data Release Products
- Daddi E., Alexander D.M., et al. 2007, *ApJ*, 670, 173
- Dale D. A. & Helou G. 2002, *ApJ*, 576, 159
- Della Ceca R., Caccianiga A., et al. 2008, *A&A*, 487, 119
- Donley J. L., Rieke G.H., Pérez-González P.G., et al. 2007, *ApJ*, 660, 167
- Donley J. L., Rieke G.H., et al. 2008, *ApJ*, 687, 111
- Donley J. L., Koekemoer A.M., et al. 2012, *ApJ*, 748, 142
- Draine B.T. 2003, *ARA&A*, 41, 241
- Elvis M., Wilkes B.J., McDowell J.C., et al. 1994, *ApJS*, 95, 1
- Fabian A.C., Iwasawa K. 1999, *MNRAS*, 303, L34
- Fiore F., Puccetti S., et al. 2008, *ApJ*, 693, 447
- Fiore F., Grazian, A., et al. 2008, *ApJ*, 672, 94
- Fazio G.G., Hora J.L., Allen L.E., et al. 2004, *ApJS*, 154, 39
- Georgantopoulos I., Georgakakis A., et al. 2008, *A&A*, 484, 671
- Glikman E., Helfand D.J., White R.L. 2006, *ApJ*, 640, 579
- Hernán-Caballero A. & Hatziminaoglou E., 2011, *MNRAS*, 414, 500
- Jarrett T.H., Cohen M., Masci F., et al. 2011, *ApJ*, 735, 112
- Lacy M., Storrie-Lombardi L.J., et al. 2004, *ApJS*, 154, 166
- Lacy M., Petric A. O., Sajina A., et al. 2007, *AJ*, 133, 186
- Magorrian J., Tremaine S., et al. 1998, *AJ*, 115, 2285
- Mateos S., Barcons X., Carrera F. J., et al. 2005, *A&A*, 444, 79
- Mateos S., Warwick R. S., et al. 2008, *A&A*, 492, 51
- Matt G. 2002, *MNRAS*, 337, 147
- Murphy K.D. & Yaqoob T. 2009, *MNRAS*, 397, 1549
- Nenkova M., Sirocky M.M., et al. 2008, *ApJ*, 685, 160
- Pineau F.-X., Motch C., Carrera F., et al. 2011, *A&A*, 527, A126
- Polletta M., Weedman D., Hönig S., et al. 2008, *ApJ*, 675, 960
- Reyes R., Zakamska N. L., Strauss M. A., et al. 2008, *AJ*, 136, 2373
- Richards G.T., Lacy M., Storrie-Lombardi L.J., et al. 2006, *ApJS*, 166, 470
- Severgnini P., Caccianiga A. & Della Ceca R. 2012, *A&A*, 542, 46
- Stern D., Eisenhardt P., Gorjian V., et al. 2005, *ApJ*, 631, 163
- Stern D., Assef R.J., Benford D.J., et al. 2012, *ApJ*, 753, 30
- Tozzi P., Gilli R., Mainieri V., et al. 2006, *AJ*, 451, 457
- Tueller J., Mushotzky R.F., et al. 2008, *AJ*, 681, 113
- Wall J.V. & Jenkins C.R., 2008, *Practical Statistics for Astronomers*, Cambridge University Press
- Watson M. G., Schröder A. C., et al. 2009, *A&A*, 493, 339
- Winter, L.M., Mushotzky R.F., et al. 2009, *ApJ*, 690, 1322
- Wright E. L., Eisenhardt P. R. M., Mainzer A. K., et al. 2010, *AJ*, 140, 1868
- Yaqoob T., Murphy K.D., et al. 2010, *MNRAS*, 401, 411